IUST Iran University of Science and Technology
Iranian Journal of Electrical and Electronic Engineering
Journal Homepage: ijeee.iust.ac.ir

Novel Turnstile Junction-Based Wideband Ortho-Mode Transducer with Stepped Tuning Stub for Ka-Band SATCOM

Lingala Srinivas*, Sunil Singarapu[*CA]

Abstract: This paper presents the design, fabrication, and analysis of a novel turnstile junction-based wideband orthomode transducer (OMT) for Ka-band satellite communication (SATCOM) systems. The proposed OMT integrates a four-stepped cylindrical tuning stub along with optimized E-plane and H-plane bends and an advanced power combiner, significantly enhancing impedance bandwidth, minimizing return loss, and improving polarization isolation-crucial for dual-polarized communication. The incorporation of this stepped tuning strategy provides improved broadband impedance transformation, enabling wide bandwidth operation, low insertion loss, and strong polarization isolation within a manufacturable architecture. Experimental validation demonstrates excellent performance, achieving a return loss better than -30 dB over 17 GHz to 34.6 GHz, isolation exceeding -60 dB, and a low insertion loss of less than 0.18 dB, with a fractional bandwidth of 68.21%. The measured results closely align with simulations, with minor discrepancies attributed to fabrication tolerances. Compared to conventional OMTs, the proposed structure offers superior electrical characteristics, reduced insertion loss, and improved polarization purity, making it a highly efficient and scalable solution for next-generation Ka-band SATCOM applications.

Keywords: Ortho Mode Transducer (OMT), turnstile junction, Ka-band SATCOM, Isolation, Return loss, Insertion loss.

1 Introduction

Satellite communication (SATCOM) has become a critical component of global connectivity, supporting applications such as broadband internet, television broadcasting, and secure military communications [1], [2], [3]. With the growing demand for higher data rates, SATCOM systems are increasingly shifting to higher frequency bands, particularly the K-/Ka-band (17.7–21.2 GHz downlink, 27.5–31 GHz uplink), which offer enhanced power efficiency and spectrum availability [4], [5]. However, operating at these frequencies presents challenges such as increased free-space loss, atmospheric attenuation, and interference, necessitating advanced system design for reliable communication [6], [7]. A key component in Ka-band SATCOM systems is the Orthomode Transducer (OMT), which enables efficient polarization separation in dual-polarized systems, minimizing crosstalk and optimizing signal integrity. The OMT plays a crucial role in improving bandwidth, reducing insertion loss, and ensuring high polarization isolation factors essential for high-capacity, interference-free communication [8], [9]. This paper presents a novel turnstile junction-based OMT with an optimized tuning stub, designed to enhance impedance bandwidth, reduce signal reflection, and achieve superior performance for next-generation SATCOM applications.

One of the earliest OMT configurations, introduced in the 1956s [10], utilized a side-coupled waveguide with a longitudinal slot, laying the foundation for modern OMT designs. Over time, OMTs have become integral to front-end feed systems requiring dual polarization [11], ensuring efficient signal separation with minimal interference. Various standard waveguide-based OMT configurations have since been widely implemented, particularly in millimeter-wave receivers for radio astronomy applications, where high isolation and low-loss performance are critical [12], [13]. Among the most recognized designs are the Boifot junction [14], [15],

[1]Iranian Journal of Electrical & Electronic Engineering, YYYY.
Paper first received DD MONTH YYYY and accepted DD MONTH YYYY.
*The authors are with the Department of Electronics and Communication Engineering, Chaitanya Deemed to be University, Hanmakonda, Telangana, India.
E-mail: sunil.ece@chaitanya.edu.in.
Corresponding Author: Sunil Singarapu.

[16], turnstile junction [4], [17], [18], [19], [20], [21], [22], [23], [24] and reverse-coupling structures [25], [26], each offering distinct operational characteristics. Moreover, [18] demonstrated excellent isolation and return loss across the K-band. However, its turnstile junction, composed of four intersecting blocks along the circular waveguide axis, poses alignment challenges, making it difficult to scale at higher frequencies. To overcome this, we propose a three-block stacked design, simplifying fabrication while maintaining superior performance. A key advancement in our design is the separate examination and optimization of the transmit and receive chains, ensuring tailored impedance matching and minimal signal degradation in each path. The transmit chain is engineered to maximize power transfer while minimizing reflection losses, whereas the receive chain is optimized for high isolation and low noise, preserving signal integrity. This refined approach enables precise machining of the waveguide's cylindrical input and the newly integrated matching stub. Utilizing CNC milling, our design achieves high structural accuracy and robustness, making it highly suitable for high-frequency SATCOM applications.

Recent advancements in millimeter-wave OMT designs have extended bandwidth capabilities, surpassing standard frequency allocations [16], [27]. However, their performance remains limited by the single-mode bandwidth constraint of conventional waveguides. For instance, [27] demonstrates a quasi-octave bandwidth (10–20 GHz) with a three-layer OMT, achieving a return loss of 25 dB, an insertion loss of 0.2 dB, and isolation of 50 dB. In comparison, the OMT proposed in this study outperforms these results by incorporating improved E, H, power combiners (E plane Tee) along with a new matching stub, which further enhances bandwidth, reduces reflection, and improves polarization isolation. This innovative approach allows for better overall performance, making the proposed OMT highly suitable for high-performance millimeter-wave applications.

In another design, a subset of Boifot-based OMTs, such as double-ridge waveguide OMTs [16], [28], [29], employs an internal double-ridge waveguide step transition. This configuration functions as a partial septum for one polarization while acting as a reduced-height waveguide transition for the other. Though compact and proven, this design restricts the ridges to the interior section while retaining standard waveguide profiles elsewhere for machinability. Consequently, its bandwidth remains confined to the single-mode limit of traditional waveguides.

Furthermore, planar OMTs have been employed at millimeter-wave frequencies to realise octave-spanning bandwidths, particularly in applications requiring on-chip integration, such as kinetic inductance detectors [30], [31], [32]. However, when a purely waveguide-based solution is necessary for lower losses and independent component testing, quad-ridge waveguide OMTs become essential for achieving bandwidths exceeding an octave. While extremely broadband quad-ridge OMTs have been developed using coaxial probes coupled.

with quad-ridge feed horns, fabrication challenges arise at frequencies beyond 10 GHz due to the stringent tolerance requirements [31], [33], [34], [35]. Additionally, some quadridge OMTs leverage turnstile junctions to enhance performance, as demonstrated in certain designs operating between 1.7–5.8 GHz [35]. However, maintaining precise mechanical clearances between features, such as ridges, turnstile stubs, and waveguide walls, poses significant manufacturing complexities.

Further advancements in turnstile-based quad-ridge OMTs have extended operational frequency ranges from 6-19 GHz to as high as 18–45 GHz [36], [37]. Some designs have incorporated modular assembly techniques, where the OMT body is fabricated in multiple segments to facilitate CNC machining. These approaches, while effective, introduce challenges in ensuring structural integrity, minimizing assembly-related losses, and maintaining tight tolerances at millimeter-wave frequencies. Similarly, commercially available wideband OMTs using WRD650 waveguides have demonstrated high insertion losses and manufacturing difficulties [8], [38].

Several high-performance turnstile-based OMTs have been reported in the literature, including the conventional design of [18], the three-layer platelet configuration of [27], and the quad-ridge implementation of [23]. In comparison, the present work adopts a multi-step cylindrical tuning structure and optimized stepped H-plane and E-plane transitions to enhance broadband impedance matching within standard waveguide operation for Ka-band SATCOM applications. Unlike ridge-based approaches, the proposed design maintains structural simplicity while achieving wide fractional bandwidth through a compact three-block stacked architecture. Therefore, the contribution is positioned as a practical and incremental refinement of turnstile-based OMT design for wideband Ka-band systems.

Alternative implementations, such as finline OMTs utilizing resistive fins to suppress higher-order modes, have shown promising results but suffer from significant trapped modes affecting cross-polarization performance [39]. Likewise, novel configurations employing magic-T junctions and coaxial probes have achieved good return loss and isolation characteristics, with potential scalability to higher frequencies [40]. Despite these advancements, designing compact, low-loss, and broadband OMTs remains a challenging task, particularly at millimeter-wave and Ka-band frequencies.

In this paper, we present a novel OMT design based on a turnstile junction, incorporating improved E, and H bends, a power combiner along with a new tuning stub to enhance impedance bandwidth. Turnstile junction-based OMTs offer a highly efficient and compact solution for dual-polarized SATCOM systems. These OMTs employ a turnstile junction to achieve a nearly perfect separation of orthogonal polarizations with minimal cross-coupling. One of the major advantages of this approach is its ability to maintain high isolation (>60 dB) and low return loss (<-30 dB) over a wide frequency range, ensuring superior signal integrity. Additionally, the turnstile junction enables broadband operation due to its symmetric structure, making it well-suited for high-data-rate and wideband SATCOM applications.

The novelty of the proposed design includes several key features that make it well-suited for SATCOM applications:

1. The new compact design easily fits into space-limited systems, allowing for affordable and scalable manufacturing without compromising performance.
2. Achieves a 68.21% fractional bandwidth with an improved design of E, H, and power combiners along with novel matching stub to enhance impedance bandwidth.
3. With >-60 dB isolation and >-30 dB return loss across the Ka-band for SATCOM (17.7 to 31 GHz), the OMT effectively reduces leakage and interference, enhancing system efficiency by measured results.
4. The double-symmetry turnstile junction and reduced-height waveguide arms provide low-loss transmission with minimal insertion loss (< 0.18 dB), validated through experimental results at Ka-band frequencies.
5. The three-block stacked architecture improves mechanical alignment, simplifies fabrication, and enhances structural stability during assembly, making the design practically suitable for compact high-frequency SATCOM front-end systems.d
6. Advanced E-plane Tee combiner ensures minimal reflections and controlled phase distribution, with an innovative non-contacting dual-step matching element improving impedance matching and wideband operation.
7. These attributes, validated through both simulation and measurement, position of the OMT using turnstile junction as a robust, high-performance solution for next-generation SATCOM systems.

2 Design of OMT

An Orthomode Transducer (OMT), depicted in Fig. 1, is a waveguide component that separates or combines orthogonal polarizations (vertical and horizontal) within a common circular port, enabling dual-polarized signal transmission in systems like SATCOM. Physically, the OMT comprises three ports: a circular waveguide (common port) supporting two orthogonal modes and two rectangular waveguide ports (Ports 3 and 4) for single-mode outputs. Electrically, it functions as a four-port device, with the common circular port treated as two independent electrical ports (Port 1: vertical polarization, Port 2: horizontal polarization). The OMT block isolates these polarizations, routing vertical polarization (Port 1) to Port 3 and horizontal polarization (Port 2) to Port 4 via TE10-mode rectangular waveguides, ensuring minimal cross-polarization interference and isolation.

In a typical RF feed chain (Fig. 2), the OMT interfaces with dual-polarized antennas and diplexers. The antenna captures/radiates vertically (V) and horizontally (H) polarized signals, which the OMT splits into separate paths (V1, V2 and H1, H2). Each polarization is processed by dedicated diplexers, which separate transmit (TX) and receive (RX) frequency bands. For vertical polarization, the upper diplexer filters TX (f1, f2) and RX (f1, f2) bands, while the lower diplexer performs identical filtering for horizontal polarization. TX bands typically occupy higher frequencies (uplink: 27.5–31 GHz), whereas RX bands use lower ranges (downlink: 17.7–21.2 GHz). By maintaining polarization purity and enabling simultaneous dual-band operation, the OMT-diplexer system maximizes spectral efficiency, critical for high-throughput SATCOM applications. The Turnstile Junction based OMT design, modeled in CST Microwave Studio, includes three ports, as shown in Fig. 3 (a). This design is optimized to effectively handle and separate orthogonal polarizations within the Ka-band frequency range. The proposed OMT features a central circular waveguide that supports dual-polarized signals, ensuring efficient mode propagation. A turnstile junction with four symmetrically arranged rectangular waveguide arms splits circularly polarized signals into orthogonal linear polarizations, directing them to respective output ports. Circular polarization is achieved through a 90° phase shift, optimized via path length differences, E-plane and H-plane bends, and power combiners. High port isolation minimizes cross-talk, while dual-polarization capability enhances data capacity. Fig. 3(b) shows the OMT's layered structure: Layer 1 contains E-plane bends, Layer 2 houses the turnstile junction, and Layer 3 integrates the power combiner. This modular design simplifies fabrication, optimizes impedance matching, and minimizes insertion loss across the target frequency range. The simulated return loss plot of the proposed OMT, shown in Fig. 3(c), covers a wide frequency range from 17 GHz to 34.6 GHz, with an impedance bandwidth of 68.21%. The return loss remains greater than -30 dB across the entire band, indicating excellent impedance matching and minimal reflection. This ensures efficient signal transmission, making the OMT ideal for reliable SATCOM applications.

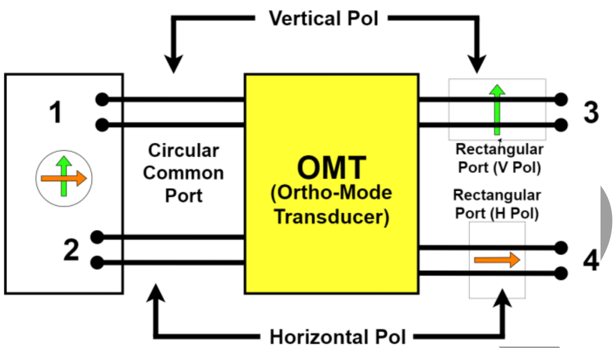

Fig. 1. Working of OMT.

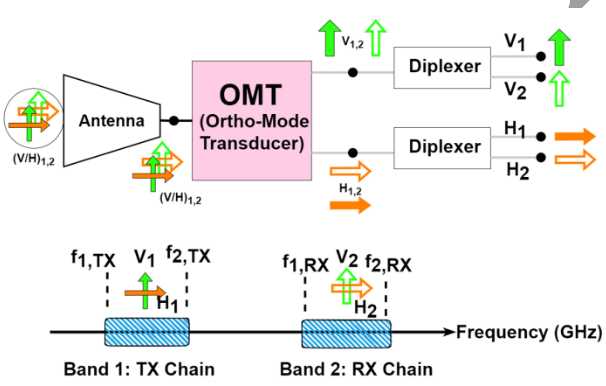

Fig. 2. Placement of the OMT in a standard RF feed network operating across dual frequency bands.

The Fig. 3(d), and Fig. 3(e) illustrate the simulated electric field (EF) distribution of the proposed OMT for horizontal (H-pol) and vertical (V-pol) polarizations. As depicted in Fig. 3(c), the TE10 mode is excited at the horizontal port, propagating through the waveguide arms while maintaining polarization purity. The EF vectors indicate minimal leakage into the orthogonal path, ensuring high isolation. The turnstile junction facilitates efficient mode conversion, reducing reflections. Similarly, as shown in Fig. 3(d), the TE10 mode is excited at the vertical port, following a distinct path while maintaining polarization integrity. The transition results in the TE11 mode at the common port, demonstrating effective polarization separation. The well-balanced field distribution ensures efficient power transfer and minimal signal distortion. The results confirm that the OMT provides high polarization isolation, optimized impedance matching, and low insertion loss. The turnstile junction and reduced-height waveguide arms contribute to stable field propagation with minimal higher-order mode excitation. These characteristics make the proposed OMT well-suited for Ka-band SATCOM applications requiring dual-polarization operation with high cross-polarization discrimination. The dimensions of the proposed OMT are given in Table 1.

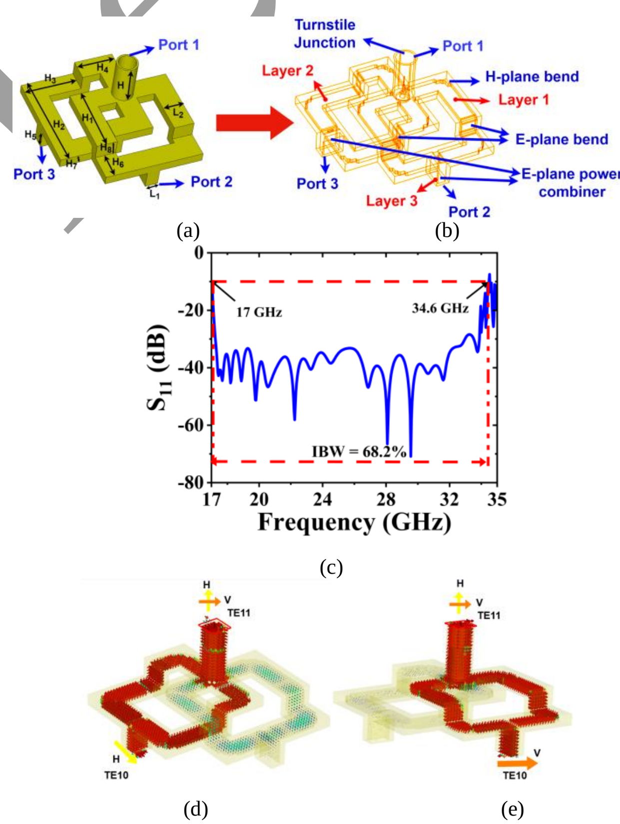

Fig. 3. (a) Proposed OMT, (b) Cross-sectional view of proposed OMT, (c) Return loss. EF distribution on OMT: (d) H-Pol, and (e)V-Pol.

Table I. Dimensions of OMT (in mm)

H	H_1	H_2	H_3	H_4	H_5
25	38	57.3	30.8	24.4	10.5
H_6	H_7	H_8	L_1	L_2	
18.6	5.2	8.9	7.3	11.8	

3. Components of OMT

An effective Orthomode Transducer (OMT) relies on key structural components to achieve high polarization isolation, low return loss, low insertion loss, and wide bandwidth. The primary elements include optimized H-plane bends, E-plane bends, and the E-plane Tee combiner, each designed to enhance signal transmission efficiency across the Ka-band SATCOM uplink (27.5–31 GHz) and downlink (17.7–21.2 GHz) frequencies. These components are simulated using CST Microwave Studio but not fabricated individually, as they are integrated into the final OMT. This section examines their design, impedance-matching mechanisms, and performance characteristics, highlighting improvements over existing OMT designs.

3.1 H-Bend with 2 steps

The 90° H-plane bend in Fig. 4(a) employs a two-step geometry (Fig. 4(b)) to minimize reflections and enhance impedance matching. The steps act as distributed tuning elements, smoothing the transition of the transverse magnetic (TM) mode through the bend. As shown in Fig. 4(c), the return loss (S11) remains below −23 dB across uplink and downlink bands, indicating robust broadband performance. This design ensures minimal signal degradation while accommodating mechanical constraints in compact OMT layouts. This two-step H-plane bend effectively minimizes reflections and enhances impedance matching. However, further improvement is achieved with a three-step H-plane bend, which provides even lower return loss and enhanced bandwidth uniformity, as discussed in the next section.

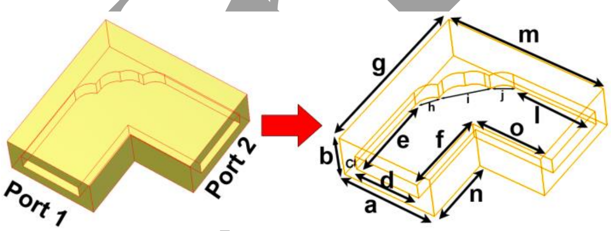

(a) (b)

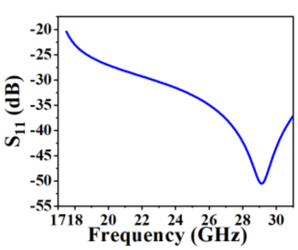

(c)

Fig. 4. (a) H-Plane bends with two steps, (b) Dimensions, and (c) S11 plot. ((a=12.85, b=6.2, c=2.2, d=8.8, e=13.16, f=11.15, g=22, h=2, i=3.5, j=3, k=1.85, l=13, m=22, n=9.15, and O=11.15) (All dimensions are in mm).

The impedance transformation employed in the H-plane bend follows the triangular tapering principle described by Pozar, where the derivative of the logarithmic impedance variation d(ln Z)/dz is triangular along the taper length. This approach minimizes reflection by distributing the impedance transition gradually. In the proposed design, the continuous triangular taper is practically implemented using discrete stepped waveguide sections. The final geometrical parameters were obtained through parametric optimization in CST Microwave Studio to achieve minimum return loss and uniform broadband performance across the Ka-band.

3.2 Improved H-Bend with 2 steps

Next, a three-step H-plane bend (Fig. 5(a–b)) improves upon the two-step design by introducing an additional step. The third step refines impedance matching, reducing return loss to below −37 dB (Fig. 5(c)). Notably, sharp dips in S11 around 17.7 GHz (downlink) and 29.25 GHz (uplink) highlight near-perfect matching at these critical frequencies. The enhanced bandwidth uniformity makes this configuration ideal for high-efficiency Ka-band systems where minimal reflection and phase distortion are paramount.

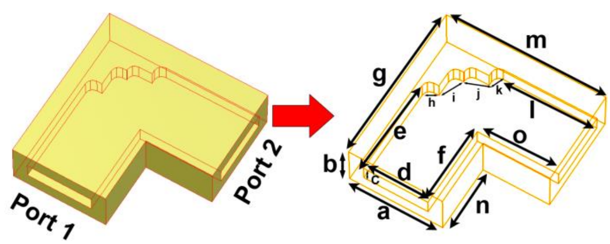

(a) (b)

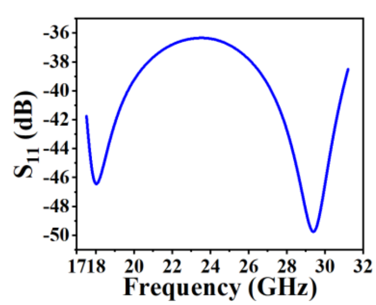

(c)

Fig. 5. (a) H bend top view, (b) Dimensions,

and (c) Return loss (dB). (a=12.85, b=6.2, c=2.2, d=8.8, e=13.16, f=11.15, g=22, h=2, i=3.5, j=3, k=1.85, l=13, m=22, n=9.15, and O=11.15) (All dimensions are in mm).

3.3 E Plane bend

The 90° E-plane bend (Fig. 6(a)) redirects the electric field vector while maintaining magnetic field orthogonality. Its optimized profile (Fig. 6(b)) achieves exceptional return loss greater than −55 dB (Fig. 6(c)). This low reflection is due to the bend's alignment with the dominant TE10 mode, ensuring minimal signal degradation and maintaining efficient wave propagation. The design's compactness and broadband efficiency make it indispensable for SATCOM systems requiring tight integration.

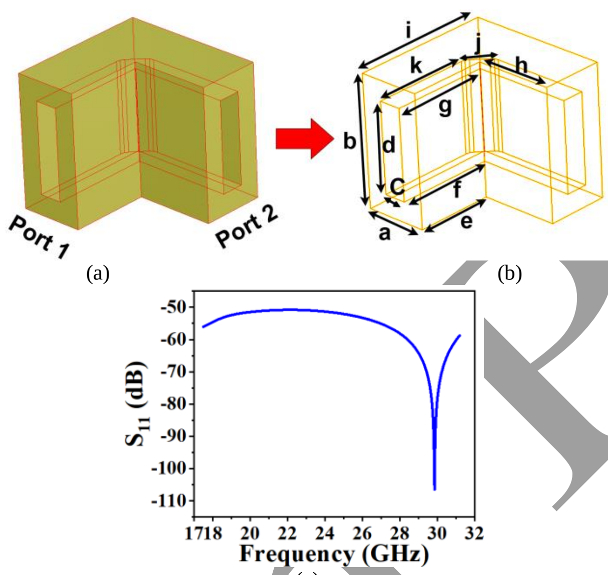

Fig. 6. (a) E plane bend, (b) Dimensions, and (c) Return loss (dB). (a=6.2, b=12.8, c=2.2, d=8.8, e=7.8, f=9.8, g=9.8, h=7.8, i=14, j=3.16, and k=9.7).

3.4 Improved E-plane Tee Combiner

The waveguide combiner (Fig. 7(a)) integrates signals from two input ports into a single output port. The optimized structure (Fig. 7(b)) ensures minimal reflections and controlled phase distribution. Fig. 7(c) presents the electric field distribution, revealing a 180° phase shift between the input ports, enabling efficient power combiner. Conventional reduced-height waveguide combiners lack mechanical compatibility with platelet OMTs, as ridges extending into adjacent layers disrupt electrical contact. To overcome this limitation, an advanced non-contacting dual-step rectangular prism matching element is incorporated at the junction of the three-port network (Fig. 7). The return loss plot in Fig. 7(d) confirms values below -35 dB across the band, ensuring optimal impedance matching and wideband operation.

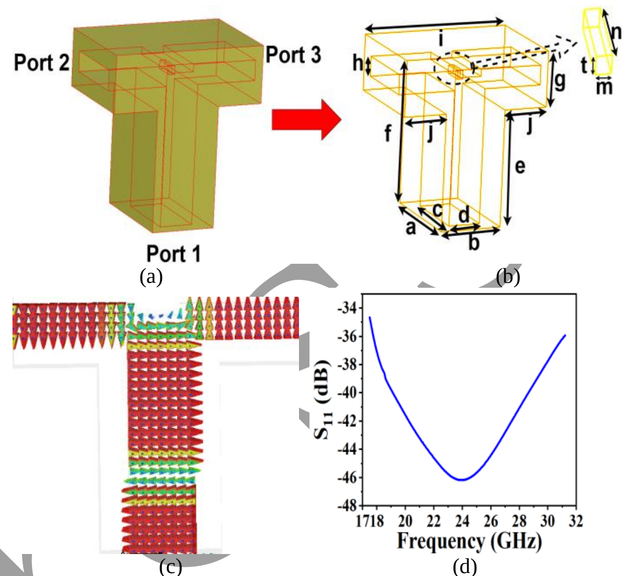

Fig. 7. (a) Combiner, (b) Dimensions, (c) EF distribution, and (d) Return loss (dB). (a=12.8, b=8.3, c=8.8, d=4.3, e=13, f=15, g=6.2, h=2.2, i=20, j=5.8, m=0.75, n=2.8, and t=0.9) (All dimensions are in mm).

3.5 Turnstile Junction

For achieving high-performance OMTs with excellent polarization isolation, it is crucial to optimize the input impedance matching at the circular waveguide by incorporating a tuning element located at the core of the turnstile junction. Several tuning configurations were evaluated and modeled to ensure optimal impedance matching across the broadest achievable bandwidth, as depicted in Fig. 8.

First, an alumina pyramid-shaped matching structure was examined, with dimensions of L = 10.8 mm and L1 = 3.8 mm, yielding a return loss of less than -25 dB. Next, a rectangular block matching step, with dimensions h = 5.6 mm and h1 = 10.6 mm, demonstrated an improved return loss of -30 dB. Further investigation was conducted using a two-stacked block-matching structure with dimensions t1 = 5.26 mm, t2 = 2.8 mm, and t3 = 0.8 mm, which resulted in a return loss of around -35 dB across the operating frequency region. However, the proposed novel four-cylindrical-tuning step-tuning structure outperforms all previous configurations, achieving an exceptional return loss of -40 dB across while simulating the entire Ka-band. This breakthrough design not only ensures minimal reflection but also significantly enhances impedance bandwidth, making it highly effective for wideband SATCOM applications. The cylindrical steps provide progressive impedance transformation, reducing abrupt discontinuities and optimizing wave propagation through the turnstile junction. The integration of this stepped tuning technique improves broadband impedance matching, contributing to enhanced bandwidth, reduced insertion loss, and improved polarization isolation. This design approach provides improved broadband performance while maintaining practical fabrication feasibility, making it well suited for high-data-rate Ka-band SATCOM systems. Fig. 9 presents the complete design of the turnstile junction simulated in CST Microwave Studio, featuring a novel four-cylindrical-step tuning structure within the branching region. This configuration is crucial for achieving superior impedance matching, high polarization isolation, and efficient signal separation in OMT systems.

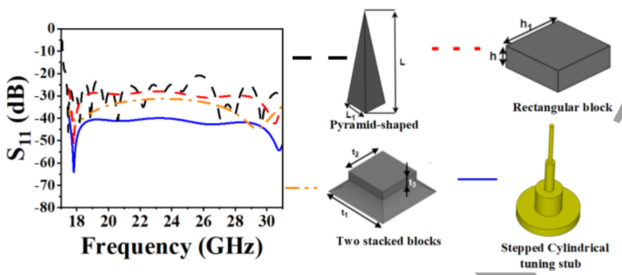

Fig. 8. Return loss for different configurations.

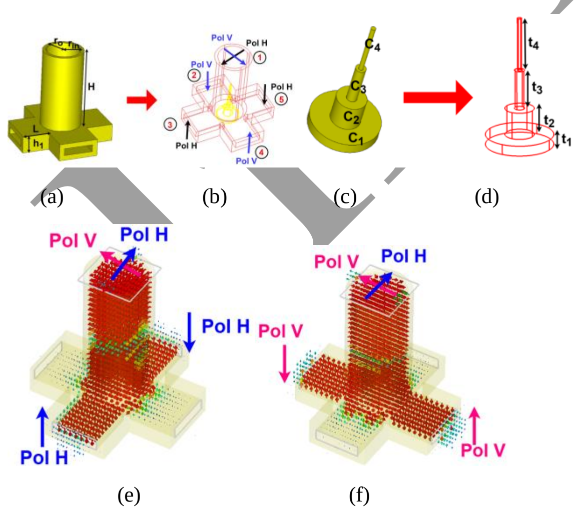

Fig. 9. Turnstile Junction. (a) Cross-sectional View, (b) Internal structure, (c) Matching element, (d) Dimensions, (e) EF-H Pol, and (f) EF-V Pol.

The geometry (Fig. 9(a)) integrates a cylindrical waveguide core with four radially connected rectangular waveguides. Fig. 9(b) presents a cross-sectional view highlighting the polarization pathways. The key innovation in this design is the four-cylindrical-step tuning structure, depicted in Fig. 9(c). This element plays a pivotal role in minimizing reflection, optimizing impedance matching, and ensuring high polarization isolation essential for dual-polarized SATCOM applications. The stepped cylinders (C1–C4), with outer radii of 3.7 mm, 1.6 mm, 0.5 mm, and 0.25 mm (Fig. 9(d)), enable gradual mode transitions, reducing abrupt discontinuities that degrade performance. The optimized cylinder dimensions are detailed in Table 2. The electric field distribution of the proposed turnstile junction is shown in Fig. 9(d) and Fig. 9(f) for H and V polarization, respectively. The four rectangular arms, symmetrically arranged around the cylindrical waveguide, form a cross-like structure. Port 1 serves as the common port, splitting incoming signals into Pol V (Ports 2 & 4) and Pol H (Ports 3 & 5) or combining them while maintaining polarization integrity. A 180° phase difference between paired ports ensures high isolation and minimal interference, optimizing performance for polarization separation and signal transmission. The scattering parameters, plotted in Fig. 10, confirm the superior performance of the proposed turnstile junction. The return loss exhibits two major dips. Two return loss minima correspond to the downlink (receive) and uplink (transmit) frequencies in Ka-band SATCOM systems. The first dip near the receive band (downlink) ensures minimal reflections, maximizing received signal power. The second dip in the transmit band (uplink) guarantees efficient power delivery to the satellite. Insertion loss remains near 0 dB, confirming negligible attenuation, while isolation remains greater than -65 dB, effectively eliminating cross-talk between channels.

Table II. Dimensions of turnstile junction (in mm)

r_o	r_{in}	H	h_1	L	t_1	t_2	t_3	t_4
6.16	5.16	23.5	5.2	8.23	1.14	3	4.4	5.96

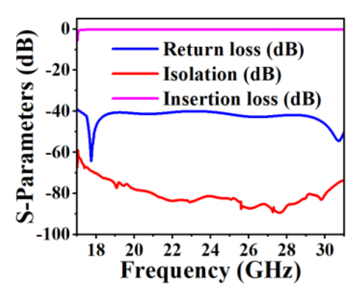

Fig. 10. S-Parameters for turnstile junction.

The stepped cylindrical tuning structure acts as a multi-section impedance transformer between the circular input and rectangular waveguide arms. Increasing the number of steps enables a smoother impedance transition, distributing reflections across multiple smaller discontinuities rather than a single abrupt mismatch. As a result, the four-step configuration provides improved broadband matching compared to two- or three-step designs while maintaining practical manufacturability.

The fourfold symmetry of the turnstile junction supports the fundamental orthogonal modes while suppressing even-mode components through differential recombination. The progressive impedance transition reduces abrupt field discontinuities, thereby limiting higher-order mode excitation and improving polarization isolation across the Ka-band.

The step dimensions were determined through parametric optimization in CST Microwave Studio. The objective function included minimizing |S11| across 17–34.6 GHz, maximizing isolation, and maintaining low insertion loss with balanced branch response. The final four-step configuration represents a trade-off between broadband performance and fabrication practicality.

Although a full statistical tolerance analysis is beyond the scope of this work, sensitivity studies performed during parametric optimization indicate that the stepped impedance configuration is less sensitive to small dimensional variations than abrupt single-step discontinuities. The symmetric architecture further enhances robustness by maintaining balanced current distribution along opposing branches.

4 Measurement results of proposed OMT

The The proposed Orthomode Transducer (OMT) is fabricated and evaluated across the Ka-band (SATCOM) frequency range, with measurements compared against simulated results for critical parameters including return loss, isolation, and insertion loss. The OMT is manufactured using precision CNC machining of aluminum alloy (Grade 6082), selected for its favorable electrical conductivity, mechanical stability, and practical suitability for high-frequency waveguide structures. Each layer is individually machined to form the required waveguide channels, junctions, and bends that support dominant-mode propagation while minimizing signal reflections. Excess material is removed where possible to reduce overall weight while maintaining mechanical robustness.

The OMT adopts a platelet-based stacked architecture, enabling compact assembly, precise alignment, and ease of integration into space-constrained SATCOM front-end systems. This innovative structure ensures efficient signal routing and supports the precision alignment required for low-loss transmission. Key components such as the turnstile junction, E-plane power combiner, and 90° H-plane bends are meticulously designed to ensure precise alignment and low-loss transitions. The assembly employs dowel pins and screws to secure layers, followed by silver plating to improve surface conductivity and environmental resilience. Fig. 11(a) and 11(b) illustrate the CST Microwave Studio-generated 3D model with three ports, while Figs. 11(c), Fig. 11(d), Fig 11(e) and Fig. 11(f) depict the fabricated OMT, comprising upper, middle, and lower blocks integrated via a monolithic turnstile junction core. The top block integrates a circular waveguide input with a transition adapter and E-plane power combiner, while the lower block houses the turnstile junction base with tuning structures and orthogonal waveguide bends. A central aluminum section bridges these layers, routing signals from the circular input to the turnstile junction and its four rectangular outputs.

A coaxial feed at Port 1 ensures symmetric signal distribution, with the turnstile junction efficiently splitting signals into orthogonal polarizations. The transmit and receive chains are optimized for high isolation and impedance matching, respectively, enabling dual-polarized Ka-band SATCOM communication with minimal reflections. To achieve circular polarization, the OMT introduces a 90° phase shift between Ports 2 and 3 through carefully engineered waveguide path differences. This phase offset ensures

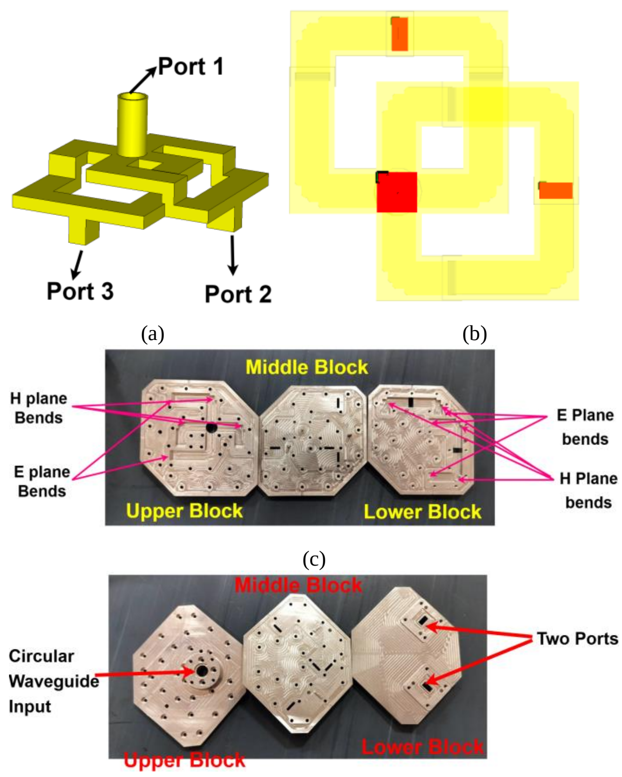

(a) (b)

(c)

(d)

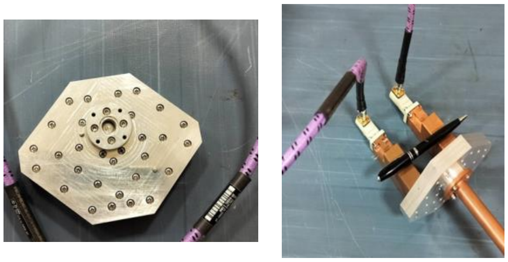

(e) (f)

Fig. 11. OMT (a) 3D view of proposed OMT, (b) Routing, Before Assembley: (c) Bottom, (d) Top view. Assembled OMT (e) Top View, and (f) Side View.

constructive interference of orthogonal modes at Port 1, yielding high polarization purity critical for SATCOM reliability. Measurement results demonstrate good agreement with simulations, though minor discrepancies arise from fabrication tolerances, connector mismatches, and unmodeled surface roughness. Return loss greater than 30 dB and isolation exceeding 60 dB across the entire band, while insertion loss remains below 0.18 dB, validating the design's efficacy. The monolithic turnstile junction, integrated with tuning structures and precision-machined components, ensures scalability to higher frequencies, making the OMT well-suited for future millimeter-wave applications, while its robust assembly and rigorous testing guarantee high signal integrity and polarization fidelity for high-performance SATCOM systems.

In SATCOM applications, both the transmit and receive chains are critical for efficient signal transmission and reception. The transmit chain (uplink) operates within the 27.5 to 31 GHz frequency range, while the receive chain (downlink) functions from 17.7 to 21.2 GHz.

4.1 Transmit Chain

Fig. 12 presents the simulated and measured S11 (dB) values for the transmit chain of the proposed OMT across the full frequency range. Both simulated and measured return loss values remain consistently below -30 dB, which is more stringent than the commonly accepted -20 dB threshold in many research studies. Both simulated and measured results show consistent performance, with discrepancies occurring at higher frequencies due to fabrication tolerances, material variations, and slight assembly misalignments. These discrepancies confirm that the OMT design closely aligns with its specifications, validating the accuracy of the simulation model.

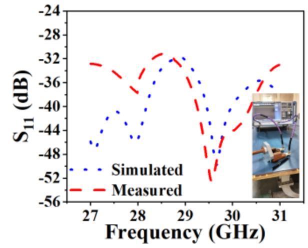

Fig. 12. Return loss in the transmit chain.

The insertion loss plot for the transmit chain (Fig. 13) remains below -0.1 dB across 27.5–31 GHz for both simulated and measured results, showing good agreement with slight discrepancies attributed to fabrication tolerances and misalignment.

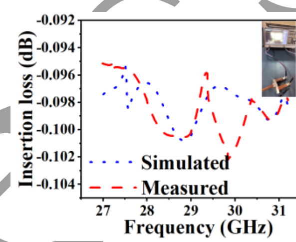

Fig. 13. Insertion loss in the transmit chain.

The S31 parameter confirms high transmission efficiency from Port 1 to Port 3, critical for Ka-band SATCOM systems to preserve signal integrity over long distances. The OMT's wideband operation and low loss, validated by consistent simulations and measurements, ensure efficient power transfer in antenna systems.

The isolation plot of the OMT, shown in Fig. 14, consistently demonstrates values below -60 dB across the 27.5 to 31 GHz range for both simulated and measured results, with minimal discrepancies. This good agreement highlights the design's reliability and accuracy, confirming that the OMT performs as expected in real-world scenarios. The measured results validate that the OMT achieves excellent isolation, ensuring stable operation and preventing interference between polarization channels in practical SATCOM applications.

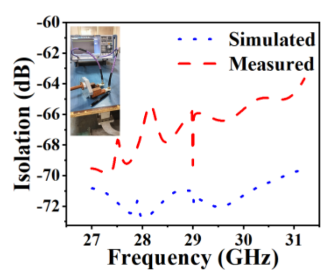

Fig. 14. Isolation in the transmit chain.

4.2 Receive Chain

Fig. 15 illustrates the return loss (S11) of the receive chain across the 17.7–21.2 GHz frequency range. The S11 values are greater than -30 dB, indicating excellent impedance matching and minimal reflection, ensuring efficient power transfer, which is ideal for Ka-band SATCOM systems. For SATCOM applications, such low reflection values are crucial, as they ensure that over 99.9% of the incident signal power is transmitted, minimizing energy loss and optimizing signal integrity.

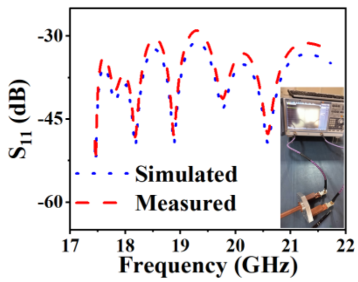

Fig. 15. Return loss in the receive chain.

Furthermore, the insertion loss (S31) performance, depicted in Fig. 16, further highlights the OMT's efficiency. The receive chain exhibits remarkably low insertion loss values of <-0.18 dB across the entire band, indicating that negligible power is dissipated within the structure. This ensures that the majority of the signal energy is retained for downstream processing, a critical requirement for maintaining high signal-to-noise ratios in SATCOM applications. The close correlation between simulated and measured insertion loss curves validates the design's accuracy and manufacturing fidelity, confirming the OMT's capability to meet stringent power transmission standards.

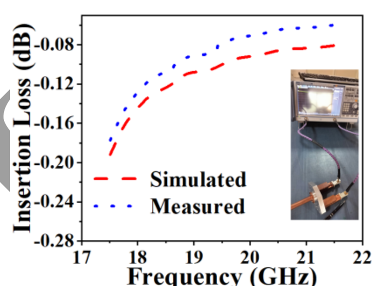

Fig.16. Insertion loss in the receive chain.

The isolation between Port 1 and Port 2 (S21), shown in Fig. 17, remains below -68 dB across the operational bandwidth. While the measured results show slightly higher values (around -60 dB), they still confirm that the fabricated OMT effectively suppresses unintended coupling. This high isolation is critical for Ka-band systems, where interference-free operation is essential for supporting concurrent high-capacity data streams. The close agreement between simulated and measured results for return loss, insertion loss, and isolation further validates the design methodology and fabrication quality of the wideband OMT.

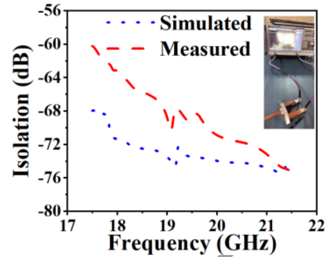

Fig. 17. Isolation in the receive chain.

5 Comparison

The proposed OMT wideband design significantly outperforms other published designs in several key performance parameters, as detailed in Table III. With a fractional bandwidth of 68.21% (17–34.6 GHz), the proposed OMT achieves superior return loss (>30 dB), insertion loss (<0.18 dB), isolation (>60 dB), and a compact volume of 30 cm³. In comparison, other designs typically exhibit lower fractional bandwidths, such as [13] (36.8%), [12] (33.33%), and [11] (31.5%), and often higher insertion losses (>0.2 dB), lower isolation values (<50 dB), and larger volumes (e.g., [13] with 120 cm³ and [11] with 80 cm³). The improved return loss and isolation in the proposed design contribute to better signal integrity and reduced cross-talk, essential for maintaining high performance in Ka-band SATCOM systems. The low insertion loss further enhances transmission efficiency, ensuring minimal signal degradation, which is crucial for long-distance communication. The compact volume of 30 cm³ also facilitates easier integration into satellite systems with space constraints, making it a more efficient and viable option compared to others with larger volumes.

Table III. Comparison of proposed work with another research.

Ref	Freq (GHz)	RL (dB)	IL (dB)	Iso (dB)	Volume (cm^3)
[13]	31-45 (36.8%)	>30	>0.2	>50	120
[12]	25-35 (33.33%)	>20	>1	>35	25
[11]	16-22 (31.5%)	>20	>0.3	>30	80
[28]	275-500 (58.06%)	>25	>0.5	>30	45
[24]	80-108 (29.7%)	>25	>0.25	>40	42
[22]	75-110 (37.83%)	>17/15	>0.5/0.6	>28	22

[9]	60-95 (45.16%)	>30	>0.2	>35	-
[27]	10-19.4 (63.9%)	>25	>0.2	>49.8	-
[29]	70-88 (22.7%)	>30	>0.25	>40	-
This work	17-34.6 (68.21%)	>30	>0.18	>60	30

Freq: Frequency, RL: Return Loss, IL: Insertion loss, Iso: Isolation.

6 Conclusion

The proposed turnstile junction-based wideband OMT demonstrates significant advancements in return loss, isolation, and insertion loss, surpassing conventional designs in key performance metrics. Fabricated and measured results exhibit good agreement with simulations, confirming the accuracy, robustness, and reliability of the design across the Ka-band frequency range. By integrating optimized waveguide components with a precisely engineered turnstile junction, the OMT achieves exceptional signal integrity, low insertion loss, and high polarization isolation, making it highly suitable for dual-polarized SATCOM applications. A key innovation in this design is the incorporation of a four-stepped cylindrical tuning stub along with improved E, and H bends, which enhances impedance matching, minimizes reflection and transmission loss, and ensures efficient power transfer over an ultra-wide bandwidth. Its compact and scalable architecture makes it particularly advantageous for space-constrained SATCOM systems, facilitating easy integration into advanced satellite payloads. Furthermore, the practical manufacturability of the design ensures cost-effective mass production, making it a viable solution for next-generation satellite communication infrastructure. With its proven high-performance characteristics, this OMT establishes a solid foundation for future advancements in wideband, high-efficiency orthomode transducers. It effectively addresses the stringent requirements of modern high-capacity SATCOM systems, ensuring low interference, superior polarization purity, and reliable operation in real-world satellite applications.

Declaration of Competing Interest The authors of the manuscript hereby declare that the above manuscript which is submitted for publication in this Journal is NOT under consideration elsewhere. the manuscript is NOT published already in part or whole in any journal or magazine for private or public circulation. All the named authors have no conflicts of interest to disclose.

Conflict of Interest: ***The authors declare no conflict of interest.***

Author Contributions:

Credit authorship contribution statement: Srinivas Lingala: Research, Writing, Editing, review, Validation. Sunil Singarapu: Validating, Editing.

Funding:

No Funding received.

Informed Consent Statement:

"Not applicable."

Declaration of generative AI and AI-assisted technologies

During the preparation of this manuscript, the authors used Grammarly to check spelling, improve grammatical correctness, and enhance English language readability. The authors reviewed and edited all suggestions and take full responsibility for the final content of the publication.

Acknowledgment

Not Applicable.

Appendix

Not Applicable.

References

[1] Y. Tao, Z. Shen, and G. Liu, "Closed-form expressions for the equivalent circuit model of square-waveguide t-junctions and its application in ortho-mode transducer design," IEEE Trans. Microw. Theory Tech., vol. 58, no. 5 PART 1, pp. 1167–1174, May 2010, doi: 10.1109/TMTT.2010.2045524.

[2] A. J. Roumeliotis, C. I. Kourogiorgas, and A. D. Panagopoulos, "Optimal Dynamic Capacity Allocation for High Throughput Satellite Communications Systems," IEEE Wireless Communications Letters, vol. 8, no. 2, pp. 596–599, Apr. 2019, doi: 10.1109/LWC.2018.2881693.

[3] H. Fenech, S. Amos, A. Tomatis, and V. Soumpholphakdy, "High throughput satellite systems: An analytical approach," IEEE Trans. Aerosp. Electron. Syst., vol. 51, no. 1, pp. 192–202, Jan. 2015, doi: 10.1109/TAES.2014.130450.

[4] J. Xiao, G. Teni, H. Li, T. Ding, and Q. Ye, "A Dual-Polarized Horn Antenna Covering Full Ka-Band Using Turnstile OMT," Front. Phys., vol. 10, p. 880606, Apr. 2022, doi: 10.3389/FPHY.2022.880606/BIBTEX.

[5] A. Mahmoud, M. Ettorre, and R. Sauleau, "High-Gain Tapered Long Slot Array for Satcom Applications in PCB Technology with Folded Corporate Feed Network," IEEE Trans. Antennas

Propag., vol. 72, no. 1, pp. 343–355, Jan. 2024, doi: 10.1109/TAP.2023.3325679.

[6] T. Jaschke, H. K. Mitto, and A. F. Jacob, "K/Ka-band dual-polarized SIW-fed lens antennas for Rx/Tx integration," Int. J. Microw. Wirel. Technol., vol. 10, no. 5–6, pp. 627–634, 2018, doi: 10.1017/S1759078718000399.

[7] A. Bhutani et al., "3D metal printed Ku/Ka Band modified turnstile junction Orthomode Transducer," Asia-Pacific Microwave Conference Proceedings, APMC, vol. 0, May 2017, doi: 10.1109/APMC.2016.7931276.

[8] J. Wang, B. Du, and Y. Wu, "Wideband orthomode transducer for the Square Kilometre Array band4 single pixel feed," International Journal of RF and Microwave Computer-Aided Engineering, vol. 29, no. 11, p. e21937, Nov. 2019, doi: 10.1002/MMCE.21937.

[9] G. P. Le Sage and C. D. Nantista, "Broadband, High Efficiency OMT in E-Band," IEEE Access, vol. 10, pp. 59630–59639, 2022, doi: 10.1109/ACCESS.2022.3180342.

[10] R. D. Tompkins, "A Broad-Band Dual-Mode Circular Waveguide Transducer," IRE Transactions on Microwave Theory and Techniques, vol. 4, no. 3, pp. 181–183, 1956, doi: 10.1109/TMTT.1956.1125048.

[11] N. J. G. Fonseca, "Very Compact Waveguide Orthomode Transducer in the K-Band for Broadband Communication Satellite Array Antennas," Sensors 2023, Vol. 23, Page 735, vol. 23, no. 2, p. 735, Jan. 2023, doi: 10.3390/S23020735.

[12] M. A. Abdelaal and A. A. Kishk, "Ka-Band 3-D-Printed Wideband Groove Gap Waveguide Orthomode Transducer," IEEE Trans. Microw. Theory Tech., vol. 67, no. 8, pp. 3361–3369, Aug. 2019, doi: 10.1109/TMTT.2019.2919630.

[13] D. Dousset, S. Claude, and K. Wu, "A compact high-performance orthomode transducer for the atacama large millimeter array (ALMA) band 1 (31-45 GHz)," IEEE Access, vol. 1, pp. 480–487, 2013, doi: 10.1109/ACCESS.2013.2273971.

[14] A. El Kamili, A. Tribak, J. Terhzaz, and A. Mediavilla, "OMT design based on Boifot Orthomode junctions for satellite communication applications in the Ku Band," ACM International Conference Proceeding Series, pp. 299–304, Sep. 2020, doi: 10.1145/3419604.3419605.

[15] A. M. Boifot, E. Lier, and T. Schaug-Pettersen, "Simple and broadband orthomode transducer," IEE Proceedings H (Microwaves, Antennas and Propagation), vol. 137, no. 6, pp. 396–400, 1990, doi: 10.1049/IP-H-2.1990.0071.

[16] A. Gonzalez and S. Asayama, "Double-Ridged Waveguide Orthomode Transducer (OMT) for the 67–116-GHz Band," J. Infrared Millim. Terahertz Waves, vol. 39, no. 8, pp. 723–737, Aug. 2018, doi: 10.1007/S10762-018-0503-5/TABLES/1.

[17] A. Tribak, J. L. Cano, A. Mediavilla, and M. Boussouis, "Octave bandwidth compact turnstile-based orthomode transducer," IEEE Microwave and Wireless Components Letters, vol. 20, no. 10, pp. 539–541, Oct. 2010, doi: 10.1109/LMWC.2010.2060261.

[18] A. Navarrini and R. L. Plambeck, "A turnstile junction waveguide orthomode transducer," IEEE Trans. Microw. Theory Tech., vol. 54, no. 1, pp. 272–277, Jan. 2006, doi: 10.1109/TMTT.2005.860505.

[19] P. Zhang, J. Qi, and J. Qiu, "Wideband turnstile junction coaxial waveguide orthomode transducer," International Journal of RF and Microwave Computer-Aided Engineering, vol. 27, no. 5, p. e21093, Jun. 2017, doi: 10.1002/MMCE.21093.

[20] P. Zhang, J. Qi, and J. Qiu, "Wideband turnstile junction coaxial waveguide orthomode transducer," International Journal of RF and Microwave Computer-Aided Engineering, vol. 27, no. 5, p. e21093, Jun. 2017, doi: 10.1002/MMCE.21093.

[21] G. Pisano et al., "A broadband WR10 turnstile junction orthomode transducer," IEEE Microwave and Wireless Components Letters, vol. 17, no. 4, pp. 286–288, Apr. 2007, doi: 10.1109/LMWC.2007.892976.

[22] J. Shen and D. S. Ricketts, "Compact W-Band 'Swan Neck' turnstile junction orthomode transducer implemented by 3-D printing," IEEE Trans. Microw. Theory Tech., vol. 68, no. 8, pp. 3408–3417, Aug. 2020, doi: 10.1109/TMTT.2020.2992065.

[23] D. Henke, N. Kelly, K. Marshall, I. Wevers, and L. B. G. Knee, "A Turnstile Quad-Ridge Orthomode Transducer (OMT) for Octave-Bandwidth Receiver Front-Ends (24-51 GHz)," IEEE Trans. Microw. Theory Tech., vol. 71, no. 11, pp. 4906–4921, Nov. 2023, doi: 10.1109/TMTT.2023.3267544.

[24] G. Virone, O. A. Peverini, M. Lumia, M. Z. Farooqui, G. Addamo, and R. Tascone, "W-band orthomode transducer for dense focal-plane clusters," IEEE Microwave and Wireless Components Letters, vol. 25, no. 2, pp. 85–87, Feb. 2015, doi: 10.1109/LMWC.2014.2373638.

[25] A. Navarrini, C. Groppi, and G. Chattopadhyay, “A waveguide orthomode transducer for 385-500 GHz,” Proceedings Volume 7741, Millimeter, Submillimeter, and Far-Infrared Detectors and Instrumentation for Astronomy V, vol. 7741, pp. 699–709, Jul. 2010, doi: 10.1117/12.857417.

[26] A. Navarrini and R. Nesti, “Symmetric reverse-coupling waveguide orthomode transducer for the 3-mm band,” IEEE Trans. Microw. Theory Tech., vol. 57, no. 1, pp. 80–88, Jan. 2009, doi: 10.1109/TMTT.2008.2008943.

[27] J. L. Cano and A. Mediavilla, “Quasi-octave bandwidth in-phase three-layer platelet orthomode transducer using improved power combiners,” IEEE Microwave and Wireless Components Letters, vol. 28, no. 12, pp. 1086–1088, Dec. 2018, doi: 10.1109/LMWC.2018.2874160.

[28] A. Gonzalez and K. Kaneko, “High-Performance Wideband Double-Ridged Waveguide OMT for the 275-500 GHz Band,” IEEE Trans. Terahertz Sci. Technol., vol. 11, no. 3, pp. 345–350, May 2021, doi: 10.1109/TTHZ.2021.3062451.

[29] H. Jiang et al., “Novel Double-Ridged Waveguide Orthomode Transducer for mm-Wave Application,” IEEE Microwave and Wireless Components Letters, vol. 32, no. 1, pp. 5–8, Jan. 2022, doi: 10.1109/LMWC.2021.3115163.

[30] Q. Yang et al., “A Dual-Polarized Planar Antenna Array Differentially-Fed by Orthomode Transducer,” IEEE Trans. Antennas Propag., vol. 69, no. 5, pp. 2637–2647, May 2021, doi: 10.1109/TAP.2020.3028211.

[31] A. W. Pollak and M. E. Jones, “A Compact Quad-Ridge Orthogonal Mode Transducer with Wide Operational Bandwidth,” IEEE Antennas Wirel. Propag. Lett., vol. 17, no. 3, pp. 422–425, Mar. 2018, doi: 10.1109/LAWP.2018.2793465.

[32] U. Jankovic and D. Budimir, “A fully planar substrate integrated probe-based wideband orthomode transducer,” IET Conference Publications, vol. 2018, no. CP741, 2018, doi: 10.1049/CP.2018.0427.

[33] A. Dunning, M. Bowen, and Y. Chung, “Offset quad ridged ortho-mode transducer with a 3.4:1 bandwidth,” Asia-Pacific Microwave Conference Proceedings, APMC, pp. 146–148, 2013, doi: 10.1109/APMC.2013.6695219.

[34] H. Z. Zhang, “A wideband orthogonal-mode junction using a junction of a quad-ridged coaxial waveguide and four ridged sectoral waveguides,” IEEE Microwave and Wireless Components Letters, vol. 12, no. 5, pp. 172–174, May 2002, doi: 10.1109/7260.1000193.

[35] K. Kotze, P. Meyer, and W. Steyn, “Design and Measurement of a Bandwidth Enhanced Quad-Ridged OMT,” 2022 16th European Conference on Antennas and Propagation, EuCAP 2022, 2022, doi: 10.23919/EUCAP53622.2022.9769398.

[36] P. V. Prasannakumar, M. A. Elmansouri, and D. S. Filipovic, “Wideband Decoupling Techniques for Dual-Polarized Bi-Static Simultaneous Transmit and Receive Antenna Subsystem,” IEEE Trans. Antennas Propag., vol. 65, no. 10, pp. 4991–5001, Oct. 2017, doi: 10.1109/TAP.2017.2734162.

[37] P. V. Prasannakumar, M. A. Elmansouri, and D. S. Filipovic, “Wideband dual-polarized bi-static simultaneous transmit and receive antenna system,” 2016 IEEE Antennas and Propagation Society International Symposium, APSURSI 2016 - Proceedings, pp. 1855–1856, Oct. 2016, doi: 10.1109/APS.2016.7696634.

[38] S. J. Skinner and G. L. James, “Wide-Band Orthomode Transducers,” IEEE Trans. Microw. Theory Tech., vol. 39, no. 2, pp. 294–300, 1991, doi: 10.1109/22.102973.

[39] G. Chattopadhyay and J. E. Carlstrom, “Finline Ortho-Mode Transducer for Millimeter Waves,” IEEE Microwave and Guided Wave Letters, vol. 9, no. 9, pp. 339–341, 1999, doi: 10.1109/75.790467.

[40] X. Cheng, Y. Wang, Y. Yao, T. Yu, J. Yu, and X. Chen, “Compact W-Band Septum Orthomode Transducer Based on Gap Waveguide,” IEEE Microwave and Wireless Technology Letters, vol. 33, no. 2, pp. 133–136, Feb. 2023, doi: 10.1109/LMWC.2022.3211859.

Biographies (All Authors)

Lingala Srinivas received the Degree in Bachelor of engineering Electronics and communication Engineering from Osmania University, Hyderabad, Telangana, India in 2011. Since 2013 he is working as Lecturer in Electronics and Communication Engineering, Department of technical Education, Government of Telangana, India. He completed his M. Tech in VLSI Systems Design from Jawaharlal Nehru Technological University, Hyderabad India in 2021. He is Currently Pursuing Ph.D degree with Chaitanya Deemed to be University, Hanumakonda, Warangal, India. He has about 12 years of Experience in Teaching.

Dr. Sunil Singarapu received the B.Tech. degree from Jawaharlal Nehru Technological University Hyderabad, India, in 2008 and the M. Tech. degree in Digital System and Computer Electronics from the Jawaharlal Nehru Technological University Hyderabad, India, in 2011. He completed the Ph.D. degree from Sri Satya Sai University of Technological and Medical Science, Sehore, Madhya Pradesh India in 2021. He has about 15 years of academic Experience. He has more than 30 publications in various journals and conferences at national and international level. He Received International Faculty Awards 2024 from Novel Research Academy for the **Best Senior Faculty Award** on 27th March 2024 from Puducherry, India. Ref no: NRA/BSFA/INT0113020/2024. His research interests are Image and Video Processing, Internet of Things, Dielectric resonator Antennas, Biosensing applications, Communications, Nano Materials, Microwaves, Radar Engineering, 5G devices and RF Communication. He is currently working as Associate Professor in Department of Electronics and Communication Engineering in Chaitanya Deemed to Be University, Hanamkonda, Telangana, India.